Channel Modeling for Millimeter Wave MIMO

Eric Torkildson, Hong Zhang, and Upamanyu Madhow
Department of Electrical and Computer Engineering
University of California
Santa Barbara, CA 93106, USA

***Abstract*— The large amounts of bandwidth available in the millimeter (mm) wave band enable multiGigabit wireless networks with applications ranging from indoor multimedia networking to outdoor backhaul for picocellular networks. Carrier wavelengths in this band are an order of magnitude smaller than those for existing cellular and WiFi systems, resulting in a drastically different propagation geometry. Omnidirectional transmission is essentially infeasible because of the increased propagation loss at smaller wavelengths; on the other hand, highly directive transmission and reception with electronically steerable beams can be achieved using compact antenna arrays. Thus, in contrast to the rich scattering environment at lower carrier frequencies, a small number of paths are dominant for directional mm wave links. The small wavelength also implies that spatial multiplexing gains can be obtained even in Line of Sight (LoS), or more generally, sparse scattering, environments with antennas with moderate separation. In this paper, we examine the consequences of these observations for two scenarios. The first is a lamppost-based outdoor deployment, where we model fading due to ground and wall reflections, and examine MIMO techniques for combating fading. The second is for spatial multiplexing for an indoor link, where we model the number of eigenmodes as a function of form factor, and examine the effect of blockage.**

I. Introduction

Millimeter wave communication corresponds to the next big leap in wireless technology. The large amounts of unlicensed and semi-unlicensed spectrum in this band (especially the 7 GHz of unlicensed bandwidth in the 60 GHz band), together with the development of low-cost silicon realizations of mm wave radio frequency integrated circuits, imply that commercially viable multiGigabit wireless technology is now within reach. The carrier wavelengths in this band are an order of magnitude smaller than those in existing cellular and WiFi networks. As a result, the propagation and interference characteristics are drastically different from our current experience in wireless network design, and demand new models and design approaches, both at the physical and higher layers. Our purpose in this paper is to highlight how mm wave Multiple Input Multiple Output (MIMO) channels differ from their counterparts at lower carrier frequencies. To this end, we investigate channel models for two scenarios. The first is for a typical link in a lamppost-based outdoor deployment (e.g., for a mesh backhaul), where we model fading due to ground and wall reflections, and examine MIMO techniques for combating fading. The second is for spatial multiplexing for an indoor link (e.g., for streaming high-definition television from a set-top box to a television set), where we model the number of eigenmodes as a function of form factor, and examine the effect of blockage.

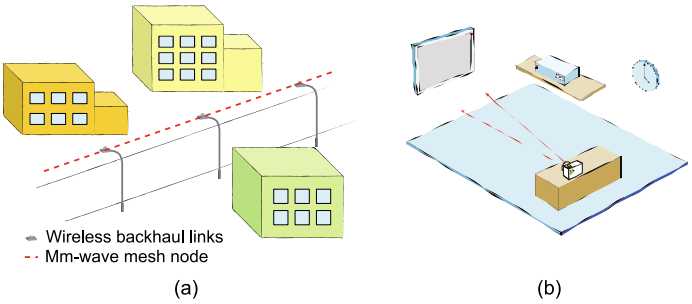

Fig. 1. The two scenarios examined include (a) a lamppost-based backhaul deployment and (b) an indoor mm-wave MIMO link.

A. Consequences of small λ

We begin with some comments on the consequences of a small carrier wavelength. The Friis formula for free space propagation implies that the path gain scales as $\lambda^2 G_T G_R$, where λ denotes the carrier wavelength, G_T denotes the transmit antenna directivity, and G_R denotes the receive antenna directivity. For fixed antenna directivities, therefore, the propagation at 60 GHz is 21 dB worse than that at 5 GHz. Since it is more difficult to generate power at 60 GHz than at 5 GHz, omnidirectional transmission is essentially infeasible for mm wave links. Fortunately, it is also a consequence of the small wavelength that it is easier to realize highly directive antennas: for a given effective area (which depends on form factor), the directivity scales as $\frac{1}{\lambda^2}$. Thus, if we fix the effective area (which essentially scales with the form factor), the overall path gain scales as $\lambda^2 G_T G_R \sim \frac{1}{\lambda^2}$, so that 60 GHz becomes 21 dB better than 5 GHz. Electronically steerable arrays of compact printed circuit antennas (again, the compactness is a consequence of the small wavelength) can be used for realizing such directional links without requiring manual pointing. As a consequence of this directivity, the multipath environment at 60 GHz is much sparser than at lower carrier frequencies (many potential paths fall outside the beamwidth of the transmit or receive antenna).

While antenna directivity leads to a sparser multipath channel, another consequence of the small wavelength is that it becomes possible to obtain a high rank MIMO channel by using multiple antennas spaced several wavelengths apart (each such antenna can be a steerable array), while still keeping the node form factor compact. Thus, spatial multiplexing can be achieved even in a line of sight (LoS) environment, rather than requiring a rich scattering environment as at lower

carrier frequencies. Yet another consequence of the small wavelength is susceptibility to blockage: obstacles such as humans look much bigger at 60 GHz than at 5 GHz. Burning through such obstacles is not a viable option (the loss due to blockage by a human can be as much as 30 dB). Thus, any 60 GHz network must have some means of avoiding, steering around, or otherwise adapting to, obstacles. This issue is most significant for indoor applications.

Finally, we make the general comment that the small carrier wavelength implies that small changes in the propagation geometry can produce drastic changes in the space-time channel.

B. Two Case Studies

In this paper, we consolidate results reported in two of our recent publications [1], [2], demonstrating the effectiveness of ray tracing for modeling the relatively sparse multipath for 60 GHz channels.

We first consider an outdoor link whose propagation geometry corresponds to a lamppost-style deployment [1]. We show that, for the directivities considered, the channel is dominated by a relatively small number of paths, corresponding to ground and wall reflections, but that small changes in ranges and heights can lead to severe fading. We also show, however, that the diversity provided by two appopriately spaced antennas (each of which may be a steerable array) suffices to combat such fading.

The second scenario [2] is an indoor link between two devices whose form factors correspond to typical electronic devices such as set-top boxes, television sets and laptops. We first note that spatial multiplexing is available even in LoS environments when antennas are separated by distances of the order of centimeters, since these correspond to several wavelengths (again, each of these antennas would typically be an electronically steerable antenna array); this is an old result, but becomes particularly relevant at small wavelengths. We then explore the limiting number of eigenmodes as a function of form factor, and show that the capacity fluctuates significantly as a function of geometry when taking into account reflections and blockage.

C. Related Work

Outdoor channel models for a city street environment, with omnidirectional antennas at 2 GHz, have been investigated in [3], [4]. However, the channel characteristics for highly directional 60 GHz links differ significantly from such models. 60 GHz mesh networks have been investigated in [5], [6], where it is shown that the design of medium access control protocols must be rethought, in order to account for the deafness and reduced interference due to directionality. However, these studies did not account for the fading caused by reflections, which is the focus of our first case study.

The capacity of an indoor 60 GHz MIMO link was previously studied in [14]. The authors considered relatively small inter-antenna spacings (2λ, where λ is the carrier wavelength) whereas in this work, we leverage prior results showing that a larger antenna separation (i.e. on the order of $\sqrt{R\lambda}$, where R is link distance) is optimal for achieving spatial multiplexing gains over a LoS channel [15]. Additionally, greater emphasis is placed on illustrating link performance as a function of node position within the environment.

II. Modeling an outdoor "LoS" link

In an outdoor urban environment, we characterize the received signal power and the channel capacity of a SISO system and a 2×2 MIMO system using a ray-traced channel model. It is demonstrated that the 2×2 MIMO system achieves robust performance, solving one of the fundamental issues of building an outdoor millimeter wave network.

A. Outdoor channel model and properties

1) Environment geometry: We consider a typical link for a lamppost-based deployment, with transmitter and receiver placed on lampposts located on one side of a straight road. It is assumed that there are buildings higher than the lampposts along the street, which contribute to multipath reflections. This assumption corresponds to a worst-case scenario: the absence of the high buildings along the street results in fewer reflected rays, which in turn causes smaller fading effects. The geometry is depicted in Fig. 2: (a) d_{wall} (wall distance) denotes the distance between the reflected building and the lamppost, (b) l is the width of the street, (c) d_s denotes the propagation distance, (d) θ_i and α_i denote the incident angle and the direct angle (the complementary angle of θ_i), respectively. Our model also includes the ground reflection (not shown in the figure).

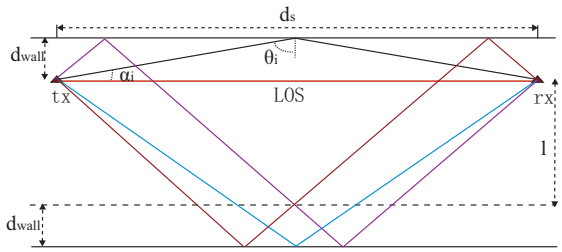

Fig. 2. Top-down view of outdoor propagation geometry illustrating LoS and wall reflected paths up to the second order.

2) Link budget and antenna design: With the assumption that the vacuum-material interface is smooth and infinite, the perpendicular and parallel reflection coefficients can be calculated from the corresponding Fresnel reflection formulas [7].

For our nominal link parameters, we consider 2 Gbps QPSK link over a distance of 200 m with 1.5 GHz bandwidth. Without fading, for an uncoded Bit Error Rate (BER) of 10^{-9}, the transmit power must be higher than 24 dBm, assuming antenna directivities of 20 dBi, a link margin of 10 dB, and a receiver noise figure of 5 dB. Rain attenuation [8] is not considered here, as our focus is on modeling multipath fading.

Antenna Design: One possible approach to obtain a 20 dBi antenna directivity is to employ a linear array of endfire antenna elements with 40° horizontal beamwidth, 30° vertical

beamwidth and half-wavelength spacing. For our numerical results, we use the radiation pattern for a printed circuit antenna built at UCSB [9] for each antenna element.

3) Six-ray Channel Model: Only reflected rays with relatively small direct angles (see Fig. 2) contribute significantly to the strength of the received signal. Consider the following parameters as an example: street width (l) of 12 m, wall distance (d_{wall}) of 4 m, the lamp post height h_{ant} of 5 m, and propagation range (d_s) of 200 m. Since the horizontal beamwidth of the transmit and receive antennas is only 10° in our scenario, it is sufficient to consider the building reflections upto the 2nd order, where the order is defined as the number of reflections impinging on the wall before reception.

As a consequence, the six-ray channel model considered in this paper includes the LoS path, the ground reflected ray, and 1st and 2nd order wall reflected rays from buildings on both sides of the road. The complex baseband representation of the received signal can be written as [10]

$$r(t) = \frac{\lambda}{4\pi}\left(\frac{\sqrt{G}u(t)e^{-j2\pi d_s/\lambda}}{d_s} + \sum_{i=1}^{5}\frac{R_i\sqrt{G_i}u(t-\tau_i)e^{-j2\pi d_i/\lambda}}{d_i}\right) \quad (1)$$

where $u(t)$ denotes the complex baseband transmit signal, $\sqrt{G}$ is the product of the transmit and receive antenna field radiation patterns for the LoS path, and $\sqrt{G_i}$ denotes the product of such patterns along the i^{th} reflected paths, d_s and d_i are the length of the LoS path and the i^{th} reflected path respectively, R_i is the product of the net reflection coefficients along the i^{th} path and the delay spread $\tau_i = (d_i - d_s)/c$ denotes the difference in propagation delay between the LoS path and the i^{th} reflected ray.

In order to focus on the effect of spatial geometry, we assume that the transmitted signal is narrowband relative to the channel coherence bandwidth (this would be true, for example, for each subcarrier in an OFDM system). Thus, we use the approximation $u(t-\tau_i) \approx u(t)$, and obtain the following expression for the received signal power:

$$P_r = P_t\left(\frac{\lambda}{4\pi}\right)^2\left|\frac{\sqrt{G}}{d_s} + \sum_{i=1}^{5}\frac{R_i\sqrt{G_i}e^{-j\triangle\phi_i}}{d_i}\right|^2 \quad (2)$$

where $\triangle\phi_i = 2\pi(d_i - d_s)/\lambda$. Fig. 3 demonstrates that the received signal power fluctuates drastically for large transmission ranges as a consequence of the destructive combination of the reflected rays and the LoS ray.

4) Statistical Distribution of the Received Signal Power: In the previous discussion, the received signal was analyzed under the assumption of the static geometry environment, which means that the antenna heights and wall distances are both fixed. However, in practice, wall distances and antenna heights inevitably vary significantly across different network deployments. Spatial variations on the order of centimeters are inevitable, and could contribute to significant fluctuations of signal strength due to the small wavelength. We use the same setting in the previous running example: the transmission range $d_s = 200$m and the street width $l = 12$m. In Fig. 4, the Cumulative Distribution Functions (CDF) of the received signal strength are plotted as either the antenna height or wall distance is randomly selected over the interval [5m,8m] or [4m,20m], while the other is fixed. This figure demonstrates that, with a relatively high probability, the received signal power exhibits significant fades below $P_{r,fs}$ (the received power in the free space propagation).

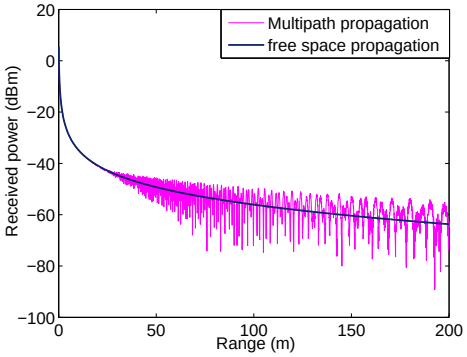

Fig. 3. Received signal power of the SISO channel as a function of the transmission range

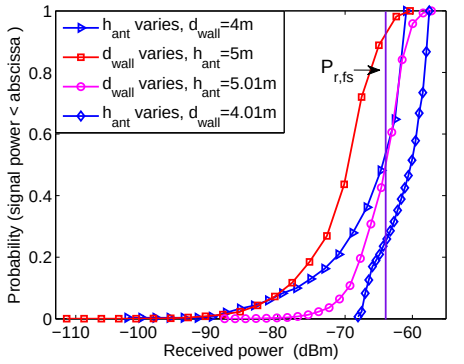

Fig. 4. CDF of received signal power of the SISO channel

The previous results state that the spatial diversity is essential to provide a robust link for the envisioned 60 GHz mesh network. In the next subsection, we show that a 2×2 MIMO system with an appropriate node geometry can be employed for this purpose.

B. MIMO diversity

We now investigate a 2×2 MIMO system. We utilize Shannon capacity as a benchmark to illustrate the performance gains relative to the SISO system, while noting that there are significant challenges in the design of multiGigabit signal processing architectures that would approach these capacities. Under the same narrowband signal assumption, the spatial channel can be expressed as:

$$\mathbf{y} = \mathbf{H}\mathbf{x} + \mathbf{w} \quad (3)$$

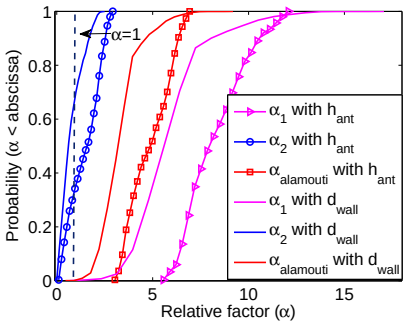

Fig. 5. CDF of the Relative Power of 2×2 MIMO channel

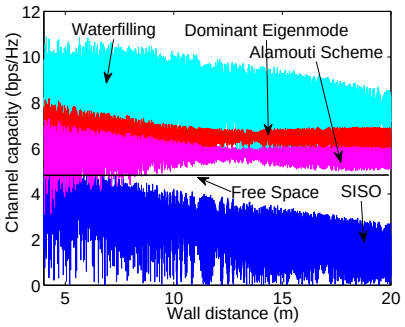

Fig. 6. Variation of channel capacity with the wall distances

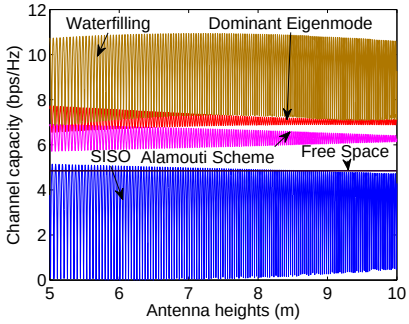

Fig. 7. Variation of channel capacity with the antenna heights

where (1) $\mathbf{y}$ is the 2×1 received signal vector, (2) $\mathbf{H}$ denotes the 2×2 channel matrix, (3) $\mathbf{x}$ represents the 2×1 transmitted signal vector and (4) $\mathbf{w}$ denotes the 2×1 additive white complex Gaussian noise vector with covariance matrix $\mathbf{C}_w = \begin{bmatrix} N_1 & 0 \\ 0 & N_2 \end{bmatrix}$. The elements of the channel matrix are calculated using ray tracing with the six ray model discussed earlier. We find that roughly 5λ separation between the two antennas along the horizontal and vertical axes works well (the horizontal separation provides diversity against the wall reflections, while the vertical separation provides diversity against the ground reflection).

1) Numerical Results: We compute the received signal power and channel capacity for three standard strategies: waterfilling [11], the use of the dominant eigenmode transmission [10] and the Alamouti space-time code [12] in the following discussion.

Received Signal Power: In order to quantify the performance gain of the MIMO system, we compare the channel capacity of the MIMO system with that of free space propagation case by defining the *Relative Power* α as: $C = \log_2(1+\alpha SNR_{fs})$, where SNR_{fs} is the corresponding SNR with free space propagation. The Relative Power is shown in Fig. 5, where α_1 and α_2 denote the Relative Powers for the corresponding channel with the first or second eigenmode respectively, $\alpha_{alamouti}$ represents the Relative Power using the Alamouti code. We note that the relative powers of the dominant eigenvalue (α_1) and the Alamouti ($\alpha_{alamouti}$) are much higher than 1 (i.e., than the power is higher than in a nominal SISO system without multipath) under variations of either antenna height or wall distance. Since the relative power of the second eigenvalue (α_2) is smaller than 1, a waterfilling algorithm utilizing both channels might achieve smaller received power relative to the dominant eigenmode or Alamouti strategies, even though it attains a higher capacity.

Channel Capacity: The channel capacity of three MIMO schemes is plotted as a function of wall distance and antenna height in Fig. 6 and Fig. 7. As expected, the waterfilling scheme achieves the highest channel capacity, but it also exhibits significant fluctuations due to variations in the eigenvalue spread. The channel capacity of the SISO system with fading is much smaller than that of a nominal truly LoS SISO system, but all three MIMO schemes achieve higher channel capacity than this nominal system with high probability. Thus, two antennas appear to suffice to handle the sparse multipath in our propagation environment.

III. Indoor "LoS" Spatial Multiplexing

We turn now to an indoor environment, where we wish to see how far we can push the limits of spatial multiplexing with nodes of relatively small form factors, taking advantage of the small carrier wavelength. We begin by providing a rough bound on the spatial degrees of freedom available to a LoS MIMO link when array sizes are constrained to the dimensions of typical electronic devices. We then proceed to examine how node placement and array alignment impacts the channel capacity of an indoor mm-wave MIMO link.

A. Limits on Spatial Multiplexing Given Array Length Constraints

We consider two $\lambda/2$-spaced uniform linear arrays (ULAs). One array has length $l_T = 1/3$ m, typical of the width of a set-top box or laptop computer, while the other array is of length $l_R = 1$ m, corresponding to a display. Given that $\lambda/2 \approx 2.5$ mm at 60 GHz, the first array has $N_T = 133$ elements and the second has $N_R = 400$. Although these arrays contain an impractically large number of elements, our motivation here is to characterize the potential for spatial multiplexing in a LoS environment given array length constraints.

To determine the spatial multiplexing capability of these arrays in a purely LoS channel, we calculate the singular values of $\mathbf{H}_{\text{LoS}} \in \mathbb{C}^{N_R \times N_T}$, the LoS channel matrix. The (m,n)th entry of $\mathbf{H}_{\text{LoS}}$, representing the (normalized) complex gain from the nth transmit antenna to the mth receive antenna, is given by

$$h_{LoS}(m,n) = \frac{p_{LoS}(1,1)}{p_{LoS}(m,n)} e^{\left(-i\frac{2\pi}{\lambda}p_{LoS}(m,n)\right)} \quad (4)$$

$$\approx e^{\left(-i\frac{2\pi}{\lambda}p_{LoS}(m,n)\right)} \quad (5)$$

where $p_{LoS}(m,n)$ is the path length between the nth transmit antenna and mth receive antenna. The normalization constant $p_{LoS}(1,1)$, though unnecessary here, is used in later simulations.

The singular values of $\mathbf{H}_{\text{LoS}}$ are calculated as the link range varies from 0.5 m to 10 m. Broadside alignment of the arrays is assumed throughout. At every link range, we

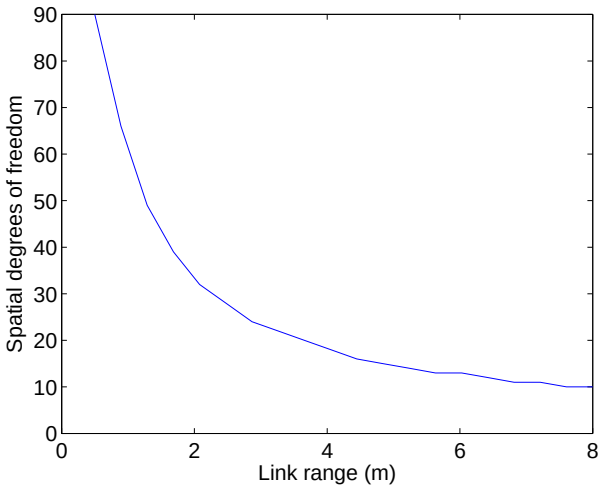

Fig. 8. Spatial degrees of freedom in a LoS environment given linear arrays of lengths $L_T = 1/3$ m and $L_R = 1$ m and a carrier frequency of 60 GHz.

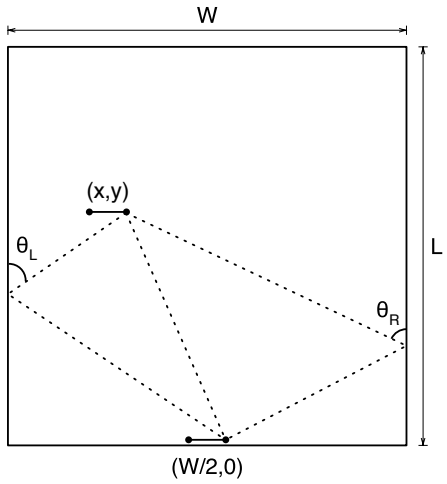

Fig. 9. Top-down view of an indoor environment illustrating LoS and single reflection paths.

observe some singular values that are orders of magnitude larger than the rest. We take the number of such singular values to be the spatial degrees of freedom, since they correspond to eigenchannels over which independent data streams can be transmitted reliably. Defining the ith singular value σ_i as dominant if $\sigma_i^2 > N_R$, Figure 8 plots the number of dominant singular values as a function of link range, assuming the two arrays are aligned to the broadside of one another. We observe at least ten dominant singular spatial degrees of freedom over the range of interest.

B. Optimal Array Configuration

The previous section demonstrated that, given array length constraints representative of typical electronic devices, significant spatial multiplexing gains are possible over a LoS channel. The arrays under consideration, however, consisted of an impractically large number of elements. Fortunately, it is possible to substantially reduce the number of antennas while preserving all available degrees of freedom. In fact, N antenna elements per array are sufficient to realize all N degrees of freedom that are available at a given range R. This is achieved by choosing the inter-antenna spacing of the N-element ULA such that $\mathbf{H}_{\mathrm{LoS}}$ is a (scaled) unitary $N \times N$ matrix. The minimum spacing that achieves this condition, assuming broadside array alignment, is given by the Rayleigh spacing criterion:

$$d_T d_R = \frac{R\lambda}{N} \tag{6}$$

where d_T is the distance between adjacent transmit array elements and d_R is the distance between adjacent receive array elements [15].

The Rayleigh spacing criterion, which maximizes the LoS channel capacity over all N-element linear array configurations, rests on three important assumptions: first, the arrays are precisely aligned; second, the link range is fixed and known *a priori*; and third, a direct LoS path between the transmitter and receiver exists. These assumptions stand in opposition to the flexibility and convenience users have come to wireless technologies, and in practice, these assumptions are unlikely to hold. This motivates us to characterize the performance of a Rayleigh-spaced array under more typical usage scenarios, i.e. when a user places the transmitter within a room at his or her convenience and when with the possibility of blockage exists. Further, the effect of multipath reflections will be incorporated into the channel model.

C. Channel Model and System Architecture

We introduce a ray tracing based channel model corresponding to the simple indoor environment depicted in Fig. 9. As shown in this top-down view, a transmitter centered at coordinates (x, y) sends data to a receiver centered on the front wall. The received vector $\mathbf{y} \in \mathbb{C}^{K\times 1}$ is given by

$$\mathbf{y} = \mathbf{B}(\mathbf{H}\mathbf{A}\mathbf{x} + \mathbf{w}) \tag{7}$$

with channel matrix $\mathbf{H} \in \mathbb{C}^{N_R \times N_T}$, precoding matrix $\mathbf{A} \in \mathbb{C}^{N_T \times K}$, spatial equalization matrix $\mathbf{B} \in \mathbb{C}^{K \times N_R}$, transmitted signal vector $\mathbf{x} \in \mathbb{C}^{K\times 1}$, and additive white complex Gaussian noise vector $\mathbf{w} \in \mathbb{C}^{K\times 1}$ with covariance $\mathbf{C}_{\mathbf{w}} = N_0\mathbf{I}_K$, where $\mathbf{I}_K$ is the $K \times K$ identity matrix. The channel matrix $\mathbf{H}$ is modeled as

$$\mathbf{H} = \mathbf{H}_{\mathrm{LoS}} + \mathbf{H}_{\mathrm{R}} + \mathbf{H}_{\mathrm{L}} \tag{8}$$

where $\mathbf{H}_{\mathrm{LoS}}$, $\mathbf{H}_{\mathrm{R}}$, and $\mathbf{H}_{\mathrm{L}}$ are the contributions of the LoS path, right wall reflected path, and left wall reflected path, respectively. Higher order reflections are disregarded in this simulation due to the additional path loss and reflection loss they incur, as well as the directionality of the antennas to be considered.

$\mathbf{H}_{\mathrm{LoS}}$ is constructed as before, while the (m, n)th entries of $\mathbf{H}_{\mathrm{R}}$ and $\mathbf{H}_{\mathrm{L}}$ are given by

$$h_R(m,n) = \Gamma(\theta_R)\frac{p_{LoS}(1,1)}{p_R(m,n)}e^{\left(-i\frac{2\pi}{\lambda}p_R(m,n)\right)} \tag{9}$$

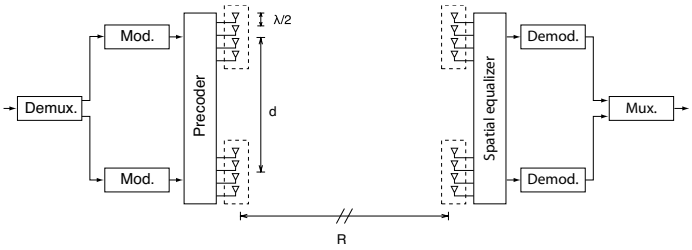

Fig. 10. Example system architecture with $K = 2$ and $M = 4$.

and

$$h_L(m,n) = \Gamma(\theta_L)\frac{p_{LoS}(1,1)}{p_L(m,n)}e^{\left(-i\frac{2\pi}{\lambda}p_L(m,n)\right)} \qquad (10)$$

respectively, where $p_R(m,n)$ $(p_L(m,n))$ is the length of the path from the nth transmit antenna to the point of reflection on the right (left) wall to the mth receive antenna. The angles of incidence off the right and left walls are given by θ_R and θ_L respectively. An expression for $\Gamma(\theta)$, the perpendicular Fresnel reflection coefficient, can be found in [7].

System architecture: The inter-element spacing of the transmit and receive arrays is set to $d = \sqrt{\lambda R/N}$ according to the Rayleigh spacing criterion with R equal to the expected link range and N equal to the number of array elements. To provide the necessary directivity, we assume each of the N elements is actually a $\lambda/2$-spaced M-antenna subarray, which, at millimeter wavelengths, could be implemented as a monolithic beamforming integrated circuit. This array-of-subarrays approach provides the necessary directivity to attenuate unwanted reflections when the LoS path is present. On the other hand, if the LoS path is blocked, the subarrays can be used to beamsteer the signal along reflected paths. The overall number of physical antenna elements per array is then $N_T = N_R = NM$. The proposed system architecture is depicted in Fig. 10 with $N = 2$.

Signals are transmitted along the N strongest eigenchannels as follows. Let the singular value decomposition (SVD) of $\mathbf{H}$ be denoted by $\mathbf{H} = \mathbf{U}\mathbf{\Sigma}\mathbf{V}^{\mathrm{H}}$, with the ordered singular values $\sigma_1 \geq \sigma_2 \geq \cdots \geq \sigma_K$ comprising the diagonal elements of Σ. $\mathbf{A}$ is then the first N columns of $\mathbf{V}$ and $\mathbf{B}$ is the first N rows of $\mathbf{U}^{\mathrm{H}}$. The rows of $\mathbf{B}$ are orthonormal, and hence the statistics of noise term $\mathbf{w}$ are unaltered by the spatial equalization process.

The channel capacity is given by

$$C = \sum_{i=1}^{N} \log\left(1 + \frac{P_i\sigma_i^2}{N_0}\right) \text{ bits/s/Hz} \qquad (11)$$

P_i is the water-filling power allocation for the ith channel given by $P_i = \left(\mu - N_0/\sigma_i^2\right)^+$, where μ is chosen to satisfy total power constraint $\sum_i P_i = P$ and a^+ is $\max(a, 0)$.

D. Numerical Results

We now compute the channel capacity assuming the proposed architecture operates in the environment depicted in Fig. 9. For simplicity, we assume two subarrays per node. The subarrays are separated by $d = 0.1$ m, which satisfies (6), the Rayleigh spacing criterion, at link range $R = 4$ m. We assume each subarray consists of $M = 5$ half-wavelength spaced antenna elements. P/N_0 is 10 dB. The dimensions of the room are 8 m by 8 m. The reflection coefficient is computed using a complex dielectric constant of $\epsilon = \epsilon_r - j\sigma\lambda$, where $\epsilon_r = 4.44$ and $\sigma = 0.001$ are chosen as suitable parameters to model plasterboard walls [14]. The receiver is centered at coordinates (4, 0) m and the capacity is calculated when the transmitter is centered at coordinates (x, y) with 0 m $< x, y <$ 8 m. The transmit array is parallel with the front wall, unless otherwise noted.

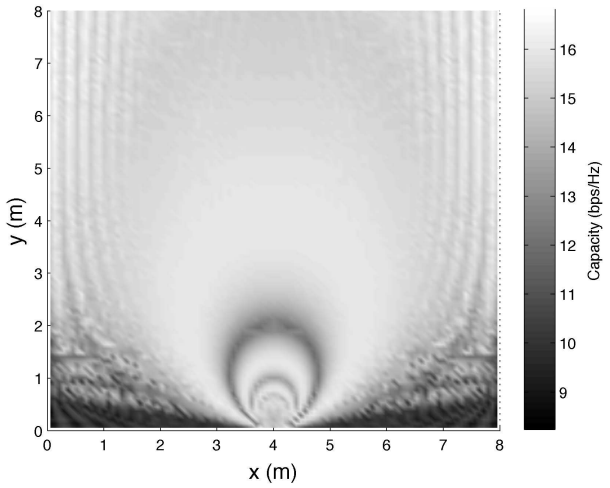

Fig. 11. Plot of channel capacity as a function of transmitter position.

Fig. 11 plots the channel capacity as a function of the transmitter coordinates. We first observe that spatial multiplexing gains boost the channel capacity throughout most of the room. Fluctuations running parallel to the side wall are a result of constructive and destructive interference of the reflected signal with the LoS signal. The reflected signal components, however, are weaker than the LoS channel component and these variations in capacity are relatively small. More significant fluctuations occur when the transmitter and receiver are brought within a close proximity of one another, which appear as a series of light and dark rings. These dips in capacity indicate an ill-conditioned channel. The receive array responses to the two transmit elements become highly correlated and spatial multiplexing gain is lost. This effect can be mitigated by adding more elements (subarrays) to the receive array [2].

We model blockage by excluding the LoS component from the composite channel matrix, i.e. $\mathbf{H} = \mathbf{H}_{\mathrm{L}} + \mathbf{H}_{\mathrm{R}}$. The transmitter and receiver beamsteer towards one (or both) reflected paths. Fig. 12 plots the capacity of the non-line-of-sight (NLoS) channel. The transmit power has been increased by 10 dB to offset the additional path and reflection losses. We observe that the channel capacity remains consistently high when the transmitter is placed in the back half of the room (4 m $< y <$ 8 m). When the transmitter is placed in the

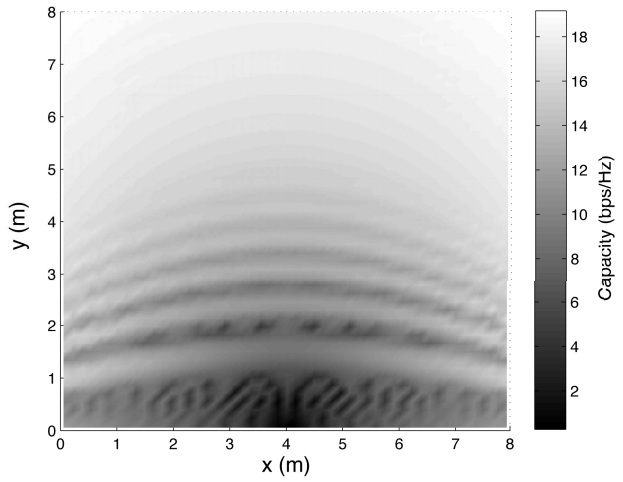

Fig. 12. Plot of channel capacity as a function of transmitter position when the LoS path is unavailable. Transmit power has been increased by 10 dB to offset reflection losses.

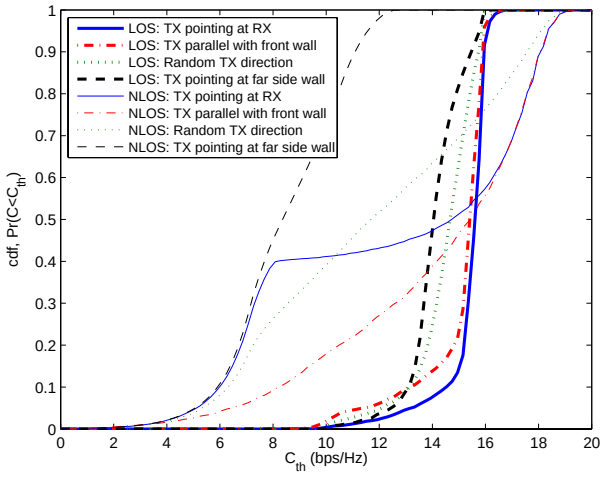

Fig. 13. CDF of the link capacity assuming random placement and various alignments of the transmit node. LoS indicates that the LoS path is available and NLoS indicates that it is blocked. The transmit power is increased by 10 dB in the NLoS cases.

front half of the room, however, the link is subject to ripple-like fluctuations in capacity that run roughly parallel to the front wall. In this case, relay nodes [16] may be useful in maintaining data throughput in the absence of a LoS path.

Fig. 13 plots the cumulative distribution function (CDF) of the capacity assuming the transmitter coordinates (x, y) are chosen at random. Several transmitter alignment scenarios are considered. In the first case, the transmit array points to the center of the receive array. This provides the best performance on average when the LoS path is unobstructed. When the LoS path is blocked, however, the near side wall often lies behind the array, and it must reflect its signal of the far side wall instead. In the second case, the transmitter is parallel with the front wall. This results in a slight decrease in LoS capacity, but provides improved performance in the non-LoS scenario because the transmitter can always reflect a signal off either side wall. In the third case, the transmit direction is a uniform random variable chosen in the range $[-90°, 90°]$ with the two extreme values corresponding to the transmitter pointing to the left and right walls, respectively. In the last case, the transmitter points to (and is parallel with) the farthest side wall. It is observed that when the LoS path is blocked, the average channel capacity is highly sensitive to array alignment.

IV. Conclusions

The two case studies here demonstrate that the propagation geometry at 60 GHz is very different from those at lower carrier frequencies. The space-time channel is well modeled by a small number of rays, so that ray tracing becomes a very effective tool. Fading is still a problem, since the channel is extremely sensitive to small changes in the environment. Our capacity computations show that multiGigabit rates are indeed possible by using channel bandwidths of the order of a GHz; in indoor environments, spatial multiplexing makes it possible, in principle, to reach 10 Gbps speeds on a 1 GHz channel. The challenge now is to realize such links, and to build effective networks based on these links. This involves answering a host of interrelated questions. How should antennas be placed on nodes for beamsteering and spatial multiplexing? How should signals be routed to and from these antennas (sending 60 GHz signals over "large" distances–relative to the wavelength–is too lossy)? How should spatial signal processing be done (at RF or baseband or a blend thereof)? How do we handle the bottleneck of analog-to-digital conversion (ADC) at multiGigabit rates (high-speed, high-precision ADC is costly and power-hungry [13])? How do adaptive mechanisms at the physical, medium access control, and routing layers interact, taking into account factors such as deafness, the overhead and efficacy of beamsteering, diversity at the node and link levels, and tradeoffs between spatial multiplexing and space division multiplexing? In short, a significant new effort in cross-layer design, starting from the physical geometry of the nodes and working up to the network layer, is required to truly exploit the potential of 60 GHz communication.

Acknowledgements

This work was supported by the National Science Foundation under grants ECS-0636621, CCF-0729222 and CNS-0832154.

References

[1] H. Zhang, S. Venkateswaran and U. Madhow, "Channel modeling and MIMO capacity for outdoor millimeter wave links," to appear in *Proc. IEEE Wireless Communications and Networking Conference (WCNC)*, Sydney, Australia, Apr. 2010.

[2] E. Torkildson, C. Sheldon, U. Madhow, M. Rodwell, "Millimeter-wave Spatial Multiplexing in an Indoor Environment," *First International Workshop on Multi-Gigabit MM-Wave and Tera-Hz Wireless Systems (MTWS'09)*, Honolulu, Hawaii, November 2009.

[3] R. Mazar, A. Bronshtern, and I.-Tai Lu, "Theoretical analysis of UHF propagation in a city street modeled as a random multislit waveguide," *IEEE Trans. Antennas Propagat.*, vol. 46, no. 6, pp. 864-871, Jun. 1998.

[4] A. A. Abouda, N. G. Tarhuni, and H. M. El-Sallabi, "Effect of antenna array geometry and ULA azimuthal orientation on MIMO channel properties in urban city street grid," *Progress in Electromagnetics Research*, PIER 64, pp. 257-278, 2006.

[5] R. Mudumbai, S. Singh, and U. Madhow, "Medium access control for 60 GHz outdoor mesh networks with highly directional links," in *Proc. IEEE INFORCOM 2009, Mini Conference,* pp. 2871-2875, Apr. 2009.

[6] S. Singh, R. Mudumbai, and U. Madhow, "Distributed coordination with deaf neighbors: efficient medium access for 60 GHz mesh networks," in *Proc. IEEE INFOCOM 2010,* March 2010, to appear.

[7] P. F. M. Smulders, "Deterministic modelling of indoor radio propagation at 40-60 GHz," *Wireless Pers. Commun.,* vol. 1, no. 2, pp. 127-135. Jun. 1994.

[8] H. T. van der Zanden, R. J. Watson, and M. H. A. J. Herben, "Rain-Induced Bistatic Scattering at 60 GHz' *EURASIP Journal on Wireless Communications and Networking* vol. 2007, doi:10.1155/2007/53203.

[9] M. Seo, B. Ananthasubramaniam, M. Rodwell, and U. Madhow, "Millimeterwave imaging sensor nets: a scalable 60-GHz wireless sensor network, " *2007 IEEE MTT-S Int. Microwave Symp. Dig.,* June 2007.

[10] A. Goldsmith, *Wireless communications.* Cambridge Univ. Press, 2005

[11] E. Biglieri, R. Calderbank, A. Constantinides, A. Goldsmith, A. Paulraj, and H. V. Poor. "MIMO Wireless Communications." Cambridge University Press, 2007.

[12] S. Alamouti, "A simple transmit diversity technique for wireless communications." *IEEE J. Sel. Areas Comm.,* vol.16, no. 8, pp. 1451-1458, Oct. 1998.

[13] R. Walden, " Analog-to-Digital Converter Survey and Analysis," vol. 17, no. 4, pp. 539-550, *IEEE J. Select. Areas Comm.,* Apr. 1999.

[14] A. Arvanitis, G. Anagnostou, N. Moraitis and P. Constantinou, "Capacity Study of a Multiple Element Antenna Configuration in an Indoor Wireless Channel at 60 GHz," *Vehicular Technology Conference, 2007. VTC2007-Spring. IEEE 65th,* pp. 609-613, April, 2007.

[15] F. Bohagen, P. Orten, and G.E. Oien, "Design of Optimal High-Rank Line-of-Sight MIMO Channels," *Wireless Communications, IEEE Transactions on,* vol. 6, no. 4. pp. 1420-1425, April, 2007.

[16] S. Singh, F. Ziliotto, U. Madhow, E. M. Belding and M. J. W. Rodwell, "Blockage and Directivity in 60 GHz Wireless Personal Area Networks: From Cross-Layer Model to Multihop MAC Design," *IEEE JSAC, Special Issue on Realizing Gbps Wireless Personal Area Networks*, 2009.